An investigation of a plug-nozzle for supersonic aircraft concepts

Khairul B.M.Q. Zaman[1], John H. Korth[2], Amy F. Fagan[3] and James E. Bridges[4]
NASA Glenn Research Center
Cleveland, OH 44135

A plug-nozzle with a cylindrical cowl is studied for thrust and noise characteristics. The geometry is adopted following commercial supersonic aircraft concepts considered in an ongoing NASA program. For the given cowl, plugs of different shapes are studied including straight conic shapes, shapes developed by a numerical optimization study for best thrust performance, as well as porous plugs. Experimental data on noise and flow field are discussed with an eye for minimum noise at low nozzle pressure ratios (NPR≈2) representing landing and takeoff (LTO) conditions. Up to NPR≈5 could be covered in the experiments. Results show that a plug designed for optimum thrust at cruise (NPR=5.9) is noisier than a plug designed for optimum thrust at LTO, over the NPR range covered. Limited thrust data with accompanying numerical simulation results are presented. Overall trend in the simulation results agree with that of the experimental results. The experiments also show that the plugs can generate transonic tones and excess broadband noise (EBBN) at low NPR, apart from the well-known screech tones and broadband shock associated noise (BBSN) at high NPR. A long porous plug is found to effectively suppress all these aberrant noise components while suffering less than 1% loss in thrust coefficient.

1. Introduction

Plug-nozzles are candidates for the exhaust system of commercial supersonic aircraft concepts in an ongoing research program at NASA [1, 2]. The exhaust system involves an 'external plug' that is an axisymmetric center-body placed concentrically near the end of the nozzle, allowing the flow to escape through the annular passage between the plug and the nozzle wall. The plug provides contoured convergence of the annular passage until the maximum plug diameter (crown) is reached near the nozzle exit. This is followed by a tapering of the plug to a point after a certain length. The pointed shape led to the use of the term 'spike' and the terminologies 'plug' and 'aerospike' have been used interchangeably in the literature.

In the early years of plug-nozzle development (1950's), two favorable observations generated keen interest. First, it was found to attain peak thrust coefficients as high as that of an equivalent C-D nozzle that has been the gold standard for propulsion efficiency with supersonic nozzle flows. Second, with a large design NPR for high altitudes, the flow was overexpanded at low altitudes; in that condition whereas a C-D nozzle suffered significant thrust losses the plug nozzle did not. Especially the latter 'altitude compensating' attribute prompted extensive research in those early years. Of course, a plug-nozzle has disadvantages that can be summed up as 'weight and heat'; the plug adds weight and being immersed in the heated flow requires cooling.

[1] Inlets & Nozzles Branch.
[2] Inlets & Nozzles Branch.
[3] Optics & Photonics Branch.
[4] Acoustics Branch.

A detailed literature review on plug-nozzles had been given in [3]. This is not repeated here for brevity. The review provided an historical account of the development of the technology starting in the 1940's and advancements over the subsequent decades. The advantages and disadvantages of plug-nozzles over C-D nozzles were discussed. The review touched upon the understanding of the flow physics for the altitude compensating attribute, as well as design of a plug by the method of characteristics for optimum thrust. Effects of plug truncation, installation effects, as well as observations on noise benefits especially with porous plugs were covered. References [4-17] are a select few out of about 60 that were invoked in the review. The last four [14-17] addressed noise aspects of plug nozzles. Possible noise benefit at LTO conditions for airport noise mitigation has been a driver for adopting the plug-nozzle in the NASA program.

As part of the program, a fundamental study is being conducted at NASA Glenn Research Center (GRC). This paper presents results from the fundamental study. Earlier results, for a plug-nozzle with a convergent aft cowl geometry, had been reported in [18]. Conventional method-of-characteristics (MoC) design for the plug requires that the flow is choked at the nozzle exit. This is why a sharp convergence of the cowl is invoked for the design in most previous studies found in the literature [5, 7, 12], leading to the choice of the convergent cowl in our earlier study [18]. Such a cowl, however, is not suitable for supersonic flights because of large boattail drag suffered by its outer surface. The boattail drag consideration dictates that the cowl be more or less cylindrical in shape.

While various other cowl shapes have been studied in the past by others (e.g., [11]), a cylindrical shape is adopted in the NASA program [19, 20]; the concept is not new and variations of such a shape had been considered before [8]. In addition to minimizing boattail drag, the cylindrical cowl shape may offer other advantages. With the plug crown located inside, the flow experiences convergence and divergence as with a convergent-divergent (C-D) nozzle. By translating the plug (or the cowl), different throat-to-exit area ratio may be achieved to obtain full expansion at different nozzle pressure ratios (NPR). This may allow a relatively easy active control strategy covering the entire flight regime from LTO to cruise conditions.

A smaller-scale model of the plug-nozzle with cylindrical cowl, following the design in the NASA program, is used for the study reported in this paper. All the plugs used with the earlier convergent cowl are readily adopted to this model. In addition, a few other plugs have been obtained following a numerical optimization study. The various plugs are investigated for noise, flow fields as well as thrust. The noise data exhibit certain unique characteristics depending on the plug shape and its axial position within the nozzle. In the following, the noise data are accompanied by schlieren flow visualization. Thrust data are accompanied by limited numerical simulation results.

This paper is a revised and extended version of the material presented in a conference paper [21]. For companion numerical simulation works on optimum plug design for the cylindrical cowl geometry and plug porosity effects please see [22] and [23], respectively.

2. Experimental Facility and Procedure

2.1 Jet facility and plug geometries

The experiments are conducted in an open jet facility at GRC [18, 21]. The experimental setup is shown in Fig. 1(a). The same setup is used to collect noise and thrust data, as well as most of the schlieren data. For thrust measurement, the flow from a 'fixed plenum', annotated on the side of Fig. 1(a), is routed through four U-shaped tubes (inner diameter = 1.31"; all dimensions in this paper are given in inches). The flow enters radially into a ‘floating plenum’ that is mounted on a linear bearing allowing it to move freely in the axial direction. Each of the four feed tubes has a flexible component. The axial force experienced by the floating plenum due to the jet exhaust is measured by a load cell attached to the face of the fixed plenum. The displacement required by the load cell is very small, within a few thousandths of an inch. Thus, the nozzle exit location remains essentially unchanged allowing the noise and schlieren measurements with the same test setup.

Since the flow enters the floating plenum radially, it has no axial force at the inlet and therefore the load cell should ideally measure axial thrust directly. However, friction, tautness of the feed tubes and other binding forces impact the measured force, hence the data reduction for actual thrust is not straightforward. A set of convergent (ASME) nozzles are used for checkout and calibration of the apparatus, as explained in section 2.2.

The flow from the floating plenum passes through two 30-mesh screens and then exhausts through the nozzle. The internal diameter of the floating plenum is 5” while the equivalent diameter of the nozzle exit is typically 1.3”; thus, the flow goes through a contraction ratio of about 15. This together with the two screens yields a uniform flow at the exit that was checked by Pitot surveys for an ASME 1.3” diameter nozzle.

The plug-nozzle is attached to the end of the floating plenum (Fig. 1a). The nozzle (cowl) has a 2” exit diameter. There is a fixed 0.75” diameter stem held centrally within the nozzle by X-shaped struts; the geometry is the same as that used earlier with the convergent cowl; an interested reader may find details in [18]. A lead screw fixed to the stem is used to attach the interchangeable plugs. A few plugs are shown in Figs. 1(b-d). Three conic plugs with half angles of 10°, 16° and 22° (denoted as ‘P10’, ‘P16’ and ‘P22’) are shown in Fig. 1(b). Whereas the plugs in Fig. 1(b) are solid, corresponding porous plugs (denoted as ‘Q10’, ‘Q16’ and ‘Q22’, respectively) are shown in Fig. 1(c). A porous plug has identical external geometry as its solid counterpart but has an internal cavity. The cavity has four quadrants separated by X-shaped struts to support the skin with pores. Some details of the 10° conic porous plug (Q10) can be seen in the CAD drawings in Fig. 1(e). The pore diameter is 0.037” and the ‘openness ratio’, i.e., the ratio of open area due to the pores to the total surface area of the skin is 6% unless stated otherwise. The plugs shown in Fig. 1(d) are discussed shortly.

Spacers placed on the internal lead screw allowed for variation of the axial location of a plug relative to the nozzle exit; the location of the plug crown (maximum diameter) relative to the nozzle exit is denoted by $\triangle$x. Also, the cylindrical section near the exit of the nozzle could be extended using lip extension pieces shown in Fig. 1(f). The extension pieces E1, E2, E3 and E4 simply fit over the end of the nozzle to extend the lip location by 0”, 0.38”, 0.74” and 1.34”, respectively.

The three plugs shown in Fig. 1(d) were designed by a numerical optimization study [22]. The plug geometry was varied by varying three parameters, L_{t1}, L and P, as shown in Fig. 2(a); *P* is a measure of the roundedness of the contour, [22]. By varying these parameters, a wide range of plug geometries could be obtained. Numerical simulation provided the thrust coefficient (*CFG*, defined in the next subsection) for each geometry for varying NPR. A design space was queried to determine the geometry yielding optimum thrust at a chosen flight condition (NPR). This way, two optimum geometries were obtained for LTO and cruise conditions. These two are ‘P38’ and ‘P39’ in Fig. 1(d) and Fig. 2(b) (referred to as ‘K1b’ and ‘K7’ in [22]). Thus, P38 has the best *CFG* at LTO condition (NPR≈2) but lower *CFG* at cruise (NPR=5.9), and vice versa for P39. Note that NPR values only approaching the cruise design condition could be covered in the facility; in fact, much of the noise and schlieren data are limited to NPR=4.6 in order maintain some safety margin. For the purposes of the present study this was considered adequate.

The third geometry, ‘P40’, (referred to as ‘K9’ in [22]), is a ‘compromise’ case yielding reasonably high *CFG* over the entire NPR range. Note that while MoC design for a convergent cowl yields a concave plug contour (‘pear’ shape), here for the cylindrical cowl the optimum plug contour turns out to be convex (‘bulged’ shape). Data from a porous plug corresponding to the P40 case, denoted as ‘Q40’, are also presented; it has similar pores as in the cases of Fig. 1(c) with 6% openness ratio.

Overhead microphones (B&K 4138) are used for measurement of radiated noise. Noise data presented in this paper pertain to a nominal microphone location of 90° to the jet axis, 45” away from the jet exit. Sound pressure level spectral analysis is performed over 0-50kHz with a bandwidth of 50 Hz, using a data rate of 100 kHz and a 50 kHz low-pass filter. The ‘jet Mach number’ M_J is defined based on the plenum pressure, p_0, and the ambient pressure, p_a, and given by, $M_J = (((p_0/p_a)^{(\gamma-1)/\gamma} - 1)\frac{2}{\gamma-1})^{1/2}$, where γ is the ratio of specific heats for air. The nozzle pressure ratio, NPR = p_0/p_a, and M_J are uniquely related to each other. These two parameters will be used interchangeably; values of both will be quoted in most cases. All data are for unheated flow, i.e., with the total temperature the same everywhere as in the ambient.

2.2 Data reduction for thrust coefficient

The performance of the thrust rig was assessed using convergent nozzles of different diameters. These nozzles have internal contours similar to standard ASME nozzles; the actual geometry can be seen in a later figure. The measured axial force (*Tm*) and mass flow rate (*mdot*), for three such nozzles with exit diameters of 1.1”, 1.3” and 1.5”, are shown in Fig. 3(a) and (b) as a function of NPR; the NPR range of 1 - 5 corresponds to the M_J range of 0 - 1.71. Data for *mdot* are obtained by an orifice-meter in the supply line. The *Tm* data are compared in Fig. 4(a) with the calculated actual thrust of the nozzles (T_{ASME}) which is obtained as follows. The ideal thrust T_{ideal} is calculated first. This is simply a function of NPR (see, e.g., [24]). It assumes uniform flow with zero boundary layer thickness. In the supersonic regime it represents the thrust had the flow expanded fully. A correlation for thrust coefficient (*CT*) for ASME nozzles, based on a large set of data, is given in [25]. This is used to determine $T_{ASME} = T_{ideal} * CT$. The force T_{ASME} would be measured had the thrust rig responded correctly. As it can be seen in Fig. 4(a) the measured force *Tm* differs from T_{ASME} due to various binding forces.

The binding force due to tautness of the feed tubes under pressure was measured by capping the nozzle while varying the pressure; this is denoted as *Tare*. The *Tare* data are also shown in Fig. 4(a). The expectation was that a correction with *Tare* would directly provide the actual thrust, i.e., $T_{ASME} = Tm - Tare$. However, for all conditions the measured *Tare* was not adequate to account for the difference between *Tm* and T_{ASME}. Furthermore, there was a small but perceptible hysteresis in *Tare* that can be seen in Fig. 4(a). The hysteresis could not be eliminated. At this point, the idea of measuring thrust directly was abandoned and an alternate method was adopted based on calibration data from the ASME nozzles.

The alternate method involved recording the difference $T_{ASME} - Tm$ as a function of NPR for the ASME nozzles, as shown in Fig. 4(b). Now, for a plug-nozzle (or any other nozzle) *Tm* and *mdot* were measured as a function of NPR. For a given NPR, the *mdot* data was used to find an equivalent diameter (D_{eq}) by interpolation of the calibration data of Fig. 3(b). The value $\triangle T = Tac - Tm$, for that D_{eq} and NPR, was then found from Fig. 4(b), where *Tac* is the expected actual thrust of the plug-nozzle. (This assumes that the annular exit area of the plug nozzle has uniform flow and an equivalent diameter of D_{eq}). *Tac* is then found as, $Tac = Tm + \triangle T$. Calculated ideal thrust provided the gross thrust coefficient as defined by, $CFG = Tac/T_{ideal}$. Note that the notation T_{ASME} is used to avoid any confusion; for an ASME nozzle $Tac = T_{ASME}$. The uncertainty in the *CFG* data was large. The repeatability of *CFG* (as measured by its standard deviation) for several sets of data for the 1.3” ASME nozzle, acquired over a day, was 0.45% and 0.7% for NPR of 4.2 and 2, respectively. This, involving scatter well over 1%, is considered large since differences within a fraction of a percent are sought to be resolved for the flows under consideration. However, the uncertainty was tighter and considered small enough for data obtained back-to-back to allow an assessment of comparative performance with parametric variations.

In the following, noise data followed by schlieren pictures for parametric variation are presented first. The effects of plug shape and porosity are discussed. In particular, the occurrence of various deleterious noise components, namely, screech tones, broadband shock associated noise (BBSN), transonic tones and excess broadband noise (EBBN), and the effect of plug porosity on them are examined. Finally, limited thrust data are discussed with corresponding numerical simulation results; the simulation procedure is briefly described with the data.

3. Results

3.1 Plug shape and crown location effect on noise and flow field

Sound pressure level (SPL) spectral data for the three optimized plugs, P38, P39 and P40 are presented in Fig. 5. Data for two nominal jet Mach numbers of 1.00 and 1.65 are shown. Recall that plugs P38 and P39 represent optimum geometries for LTO and cruise conditions, respectively, while plug P40 is a compromise case. The data in Fig. 5(a) represents a LTO condition. The crown location △x, M_J and OASPL (dB) are shown in the 2nd, 3rd and 4th columns of the legend, respectively, in this and all subsequent spectral figures. For all data in Fig. 5 the crown location is near the exit (△x= -0.035") which is the design location for the P38 plug at LTO condition (M_J ≈1). Clearly, P39, optimized for cruise with design △x smaller than -0.035, is noisier at M_J=1 (Fig. 5a). The data for off-design △x values are considered to provide a broad perspective of the noise generated by these plugs. In Fig. 5(b), BBSN, represented by the broad peak around 4.5kHz, dominates the spectra for all plugs. This peak is seen to be most pronounced for the P39 case and least for the P40 case.

Schlieren data corresponding to the cases of Fig. 5 are shown in Fig. 6. These are time-averaged images, and data for M_J =1 (NPR=1.89) and M_J =1.65 (NPR=4.6) are shown in the upper and lower rows, respectively. Shocks can be seen just past the nozzle exit at M_J =1, as the flow accelerates around the plug crown. The shock appears least pronounced for the P38 case which has a milder curvature around the crown. At the higher M_J, all three plugs exhibit a bulging flow out of the nozzle representing an underexpanded condition. This is expected since with the crown located near the nozzle exit the flow passage is essentially convergent.

For a given plug, the crown location (△x) determines the throat-to-exit area ratio. Within the experimental constraints the crown location could be varied in discrete steps. The approximate values of △x for obtaining throat-to-exit area ratios for optimum thrust at NPR of 4.6 (M_J =1.65) are △x= -0.9", -0.415" and -0.415" for the P38, P39 and P40 cases, respectively. Noise and schlieren data were acquired for the three plugs with those respective locations. Noise data are shown in Figs. 7, for M_J =1.65. It is seen that the LTO optimized plug (P38) is still least noisy (red trace). P39, designed for NPR=5.9 (M_J =1.82), is seen to produce the highest BBSN peak as well as a screech component (blue trace). The compromise case (P40, green) has an intermediate level of noise. Corresponding schlieren data are shown for in Fig. 8. These exhibit shock structures that are similar for all three plugs. Comparison with data in Fig. 6 (lower row) delineates the effect of crown location. With crown locations chosen to provide full expansion at M_J=1.65, the flows in Fig. 8 are almost parallel (cylindrical) whereas with crown location near the exit the corresponding flows in Fig. 6 were bulging outward (underexpanded). Of course, the flows in Fig. 8 are not perfectly expanded and have shocks because these are not simple convergent-divergent flows and there is the presence of the plug.

The relative crown location effect is studied with the 16° conic plug. A 16° conic plug has been used in a larger-scale NASA experiment in the past [19, 20], and is to be used in another upcoming experiment. Thus, noise and schlieren data for this plug with varying △x may be useful. Numerical simulations are also performed with this plug and comparison with experimental thrust data will be discussed in a later section. SPL spectra for the P16 plug are shown for four crown locations of -0.286", -0.665", -1.025" and -1.625", for M_J =1.05 (NPR =2, LTO) and M_J =1.65 (NPR=4.6, cruise) in Figs. 9(a) and (b), respectively. The crown locations were achieved simply using the four extensions E1, E2, E3 and E4 without any spacers. The spectral data are staggered for clarity; successive traces are shifted by 5 dB, the ordinate being pertinent to the trace at the bottom. First, at the higher M_J in Fig. 9(b) BBSN peak and screech tones are seen. The frequencies of the BBSN peak (at about 5.5 kHz) do not change significantly with varying △x. In Fig. 9(a), at M_J =1.05 (NPR=2), a large spectral peak representing a loud tone occurs for the upstream-most crown location (△x =-1.625"). This is a 'transonic tone' discussed shortly.

Schlieren pictures corresponding to the conditions of Fig. 9 are shown in Fig. 10. Instantaneous images are shown for the lower M_J in order to provide an idea about the flow unsteadiness whereas time-averaged images are shown for the higher M_J that capture the shock structures more clearly. (The time-averaged images were obtained in a later set of experiment. Some differences in the schlieren setup caused the difference in the brightness of the background). At M_J = 1.65, the shock structure appears relatively weak for the upstream-most crown location (bottom right). This is expected since with that crown location the throat-to-exit area ratio approaches the design value for full expansion. At the lower M_J of 1.0 and △x= -1.625" (bottom left), the condition of transonic tone, the flow exhibits organized large-scale vortical structures (just downstream of the plug tip). The instantaneous images were at arbitrary times and hence such structures appeared randomly.

3.2 Plug porosity effect

The effect of plug porosity on noise and flow is now addressed. Noise data for the 10° conic plug, shown first in Figs. 11 and 12, exhibit a significant effect. Pairs of spectral data are presented for the solid (P10) and the corresponding porous plug (Q10), for four values of M_J all with △x= -0.035". Large effects are noticed. BBSN and screech are effectively suppressed by the porosity. (At lower M_J and subsonic conditions practically no effect was observed, data not shown for brevity).

Corresponding schlieren data are shown in Fig. 12. A comparison of the images shows that the shock structure occurring with the solid plug (for example, at M_J =1.4) is significantly altered and weakened by the porosity. Similar data with the same plug and the convergent cowl, at same M_J, exhibited a more pronounced effect [18]. Thus, with the cylindrical cowl the plug porosity effect is somewhat less pronounced. Nonetheless, the noise suppression is still very significant.

It was anticipated that the 16° conic plug would also exhibit a similar effect of porosity on noise. A 16° plug, which is shorter and lighter than the 10° plug, is preferable from an application point of view. Unfortunately, the porosity effect with the 16° case was minimal or detrimental. An increase in noise actually occurred under certain conditions. The noise data shown in Fig. 13, illustrates this. Note the appearance of BBSN and screech for the porous case in Fig. 13(c) that was absent with the solid case. Schlieren data are presented in Fig. 14 for M_J =1.4 and 1.5 between which the effect reverses. The effect on the downstream shock structure is revealing. An organized (spatially periodic) shock structure downstream of the plug tip is seen weakened at M_J =1.4. Comparatively, a reverse effect is seen for M_J =1.5. Here, the shock structure downstream of the plug tip are seen to get re-formed when using the porous plug. The train of shocks in the downstream region of the jet is known to cause BBSN. Thus, the schlieren data is consistent with the increase in BBSN when using the porous plug at M_J =1.5. Why the shocks get organized and accentuated in the 16° case at M_J =1.5 by the porosity remains unclear at this time. Further research will be required to obtain a clearer understanding.

We note here that data taken with the 22° conic case, not shown for brevity, also exhibited an increase in BBSN by plug porosity at M_J =1.38. Other shorter plugs also exhibited contradictory effects. An example is shown in Figs. 15 and 16 for the numerically designed case (P40 vs. Q40). Here, BBSN increases with the porous plug at a lower M_J (=1.3, Fig. 15a), while it is suppressed at a higher M_J (=1.4, Fig. 15b). Corresponding schlieren data exhibit a more organized shock diamond structure caused by the porosity at M_J =1.3, (top row of Fig.16). It is vice versa at the higher M_J (1.4, lower row in Fig.16). It is emphasized here that repeat measurements with the 10° case, on the other hand, exhibited the suppression of BBSN and screech as seen in Fig. 11 consistently. Thus, a longer plug may be needed to realize the beneficial effect of porosity on noise. Thrust data also show a better thrust performance for the 10° plug relative to the shorter plugs, as well as minimal thrust loss due to the porosity, discussed shortly.

3.2.1 Transonic tone and EBBN: Recall the transonic tone observed in Fig. 9. The characteristics of these 'x-tones' and the related phenomenon of excess broadband noise (EBBN), occurring with the plug-nozzle flows, is explored using the 10° conic plug. The x-tone phenomenon was studied in [26] for convergent-divergent nozzles. It was found to occur when a shock resided within the divergent section. The unsteady shock motion locked on to a one-quarter wave acoustic mode of the divergent section to produce the intense tone. Later it was found that even in the absence of a locked-in resonance, the broadband noise levels were unusually high relative to the noise from a convergent nozzle of same throat area, at same NPR. The high noise was termed excess broadband noise (EBBN) and attributed to unsteady (random) shock motion within the divergent section [27]. The same phenomena occur with a plug-nozzle flow, when the plug crown is inside the nozzle creating a convergent-divergent passage.

SPL spectra are shown in Fig. 17(a) for a number of M_J for the 10° conic plug placed with △x= -1.625". For clarity the data are shown in a staggered pattern. With increasing M_J a tone occurs around M_J =0.53; the frequency increases with increasing M_J and then goes through a stage jump around M_J =0.86; eventually the tone ceases for M_J >1.04 for the given configuration. The frequencies of the spectral peaks (in kHz) and their amplitudes (in dB, with the given analysis bandwidth), from the data of Fig. 17(a), are shown in Fig. 17(b). The two stages of the tone can be seen. The stage on the right is recognized as the fundamental ¼-wave resonance, hence it is denoted 'stage 1'; 'stage 2' represents the third harmonic. A curious reader may find further details in [26].

The straight lines through the frequency data in Fig. 17(b) are from a correlation equation, based on C-D nozzle data, provided in [26]. In the correlation, the tone frequency, nondimensionalized by the velocity and the throat-to-exit length, is expressed as a function of the half-angle of the divergent section. For the present case an equivalent half-angle is calculated from the throat and exit areas to be 7.94° and the length-scale is taken as 1.537" which is slightly less than the throat-to-exit distance of 1.625". (Note that in the correlation equation of [26] the length-scale was simply the throat-to-exit distance. Here, the flow is through an annular passage and because of the presence of the plug the flow exit location is not well defined. An average distance of two points on the plug surface, measured from the throat, is taken as the length-scale. One of these points is the distance of the nozzle exit from the plug crown (1.625") and the other is the intersection of a line drawn from the nozzle lip and perpendicular to the plug surface (1.449"); this yielded the length 1.537"). It is seen that the correlation agrees reasonably well with the frequency data leaving no doubt that the tone observed here is the same as the transonic tone.

It should be noted here that with increasing M_J (and NPR) the threshold at which the throat becomes choked depends on the throat-to-exit area ratio. The smaller ratio, the lower is the threshold. In the present case, (equivalent diameters of throat and exit being 1.276" and 1.732"), the threshold is at about M_J =0.336 (NPR = 1.081). In Fig. 17, there is a range of M_J between the x-tone stages when there is no tone. There are also methods that eliminate x-tones [26]. However, in all cases in the absence of any tone, it was shown in [27] that the broadband noise levels were high, relative to levels expected from a convergent nozzle of same throat area at same NPR. This was denoted as EBBN. For the plug-nozzles, EBBN is examined in the context of plug porosity effect.

3.2.2 Plug porosity effect on transonic tone and EBBN: SPL spectra for the 10° plug are presented in Fig. 18 for solid (P10, red lines) and porous (Q10, blue lines) cases, at four M_J with △x=-1.625". Figure 18(a) and (b) captures the x-tone in the two stages, seen in Fig. 17. It is readily seen that the porosity completely eliminates the x-tone. Figure 18(c) shows spectra at a condition between the two x-tone stages where there is no tone. It is instructive to first compare the data for the solid plug (red line) with that from a simple convergent nozzle (grey line), that has the same throat area (1.3" diameter). The red line is 6-8 dB higher in amplitude; this difference is EBBN. Now note the effect of the porous plug; it has suppressed the EBBN and brought the levels down significantly reducing OASPL by 5.5dB. Figure 18(d) is included to show the suppression of EBBN for a different crown location of △x=-1.025"; here, OASPL has reduced by about 5dB. Schlieren pictures for the three cases with △x=-1.625" (Fig. 18c) are shown in Fig. 19. Large scale vortical structures are visible with x-tone (see the top two pictures on left column). Similar structures are also seen occasionally in the case of EBBN (bottom picture on left column). It is apparent that the porous plug (right column) has weakened the vortical structures that is accompanied by a suppression of both x-tone and EBBN. The effect likely traces to a weakening of shock(s) by the porosity within the divergent section.

Certain methods, e.g., tripping the boundary layer near the throat of a C-D nozzle was successful in suppressing x-tones [26]. However, no method had been known for suppression of EBBN. Similarly, with reference to the data in Fig. 11, there are known methods for suppression of screech tones (such as by placing a tab at the nozzle lip) but none that would suppress BBSN. The porous plug has suppressed both EBBN and BBSN in addition to eliminating screech and x-tone. It is plausible that a porous plug with a fixed crown location inside the cowl may serve to produce low noise at LTO while yielding optimum thrust at cruise. Such a fixed porous plug, rather than a translating plug requiring different crown position in different flight regime, would simplify the design as well as reduce weight. Such a possibility will require more research.

It should be mentioned here that with the shorter plugs (e.g., P16 and P40) x-tones and EBBN also occurred when the plug was placed inside the nozzle. Corresponding porous plugs (Q16 and Q40) did take out the x-tones. However, they did not suppress EBBN as much as seen in Fig. 18. The porosity effect on noise suppression occurred most significantly with the longer 10° plug. Unfortunately, the suppression was not clear and consistent with the shorter porous plugs that would have been desirable from an implementation point of view. A longer porous plug indeed may have to be considered in future designs.

3.3 Thrust data compared to CFD results

In view of the large uncertainty, discussed in section 2, only limited thrust data are presented. Some of these are accompanied by Computational Fluid Dynamics (CFD) analysis. The CFD calculations are performed using ANSYS Fluent software, assuming axisymmetric steady state and fully turbulent compressible flow of calorically perfect air, with Reynolds-averaged Navier-Stokes (RANS) model equations solved implicitly over adaptively refined unstructured meshes. Further details of the CFD analysis can be found in [22]. First, as a sanity check, *CFG*, defined in section 2.2, for the *D*=1.3" ASME nozzle is examined in Fig. 20. Experimental data and CFD data are shown by the red (solid) and the blue (dashed) curves with symbols, respectively, in Fig. 20(a). The trends and the amplitudes agree well, considering the uncertainties in the experiment as well as in the simulation.

The results in Fig. 20(a) are also compared with analytical predictions. The ratio T_{conv}/T_{ideal} is shown by the green line; T_{conv} is the calculated thrust for a convergent nozzle. Both T_{ideal} and T_{conv} assume top-hat exit velocity profile with zero boundary layer thickness. Whereas T_{ideal} assumes full expansion of the flow, T_{conv} accounts for the unbalanced pressure at the nozzle exit, in supersonic conditions. The ratio is unity in subsonic conditions (NPR < 1.89) and it decreases with increasing NPR in supersonic conditions. The solid light blue curve is the correlation *CT* for ASME nozzles from Ref. [25]; recall from section 2.2 that $CT=T_{ASME}/T_{ideal}$. Its difference from the green curve is due mostly to boundary layer losses. Ideally, the experimental and CFD results should agree with the light blue (*CT*) curve. Differences are not unexpected. Apart from data uncertainty there can be differences in the boundary layer states. (There is also considerable scatter in the data from which the correlation equations were derived in [25]). Thus, the agreement with the predictions is considered reasonable and these results, in fact, provided confidence in the present methods. The plot in Fig. 20(b) is a sample CFD data clip at NPR=4.25; calculated flow fields like this yielded the *CFG* results shown in Fig. 20(a). Figure 20(b) also shows the geometry of the *D*=1.3” ASME nozzle.

Since a 16° plug is planned to be used in an upcoming larger-scale experiment, some CFD efforts were devoted early on for this plug and compared with the experimental thrust data. Figure 21 shows experimental results compared to the CFD results corresponding to the cases shown in Figs. 9 and 10. The effect of four axial locations of the plug crown on *CFG* is shown as a function of NPR. In the sketch in Fig. 21(b), the extension E1 (△x= -0.035”) is represented by the dark blue wall; lip locations for extensions E2, E3 and E4 (△x= -0.665”, -1.025” and -1.625”)) are shown by the red, green, and grey walls, respectively. The same color code is used for the data in Fig. 21(a), where the solid lines represent experimental data, and the dashed lines represent CFD results. It is seen that the data trends as well as amplitudes agree reasonably well between the experiment and CFD. These results provided added confidence in the adopted CFD procedure that are continued and expanded to study plug-nozzles [e.g., 22, 23].

Finally, the important question of thrust loss due to plug porosity is addressed. The porosity effect on *CFG* is shown in Fig. 22, with experimental data for the 16° and 10° conic plugs and their porous counterparts. The same scales as in Fig. 21(a) are used for comparison. While a reduction in *CFG*, due to porosity, in the order of 1% is noted for the 16° case (Fig. 22a), a smaller reduction over most of the NPR range is noted for the 10° case (Fig. 22b). These results delineate that the losses in *CFG* with the presently used porous plugs are small. We have seen that the noise reductions by the 10° conic porous plug was quite significant. It suppressed not only screech tones and x-tones but also BBSN and EBBN, with less than 1% loss in *CFG*.

4. Conclusions

A fundamental study was carried out with the aim of providing recommendations for the best external plug geometries for supersonic aircraft concepts in an ongoing NASA program. To that end, numerical optimization studies provided optimum plug geometries for LTO and cruise conditions. With a cylindrical cowl these shapes turned out to be characterized by convex contours or bulges. Such shapes differ from the ‘pear’-like plug shapes with concave contours as predicted by method of characteristics for convergent cowls. The LTO and cruise conditions yielded largely different plug shapes for optimum thrust; a compromise shape was also developed with the hope that it would provide adequate performance over the full operating range. These three plug shapes were explored in the present experimental study, in addition to conic shaped plugs as well as porous plugs. Noise and flow field data were examined over a range of NPR. An emphasis was to look for geometries that would yield minimum noise at low NPR (LTO) while not sacrificing thrust at cruise.

Results show that a plug designed for optimum thrust at cruise was noisier throughout the NPR range covered. A plug designed for optimum thrust at LTO had lower noise throughout the NPR range while the compromise plug case had intermediate noise levels. The results also show that a cylindrical plug-nozzle, depending on the location of the plug crown relative to the nozzle exit, can generate transonic tones (x-tones) and excess broadband noise (EBBN) at low NPR, apart from the well-known screech tones and broadband shock associated noise (BBSN) at high NPR. A long porous plug is found to effectively suppress all these aberrant noise components while suffering less than 1% loss in thrust coefficient.

Thrust coefficient data acquired for a few cases showed good agreement with corresponding numerical simulation results. This provided confidence in the numerical methods that are being used to investigate the extensive parameter space for optimizing the plug geometry. Companion numerical results from this study are presented separately.

Acknowledgement

The work is supported by NASA's Commercial Supersonic Technology (CST) Project under NASA's Advanced Air Vehicles Program.

References

1. Berton, J.J., "Variable Noise Reduction Systems for a Notional Supersonic Business Jet", *J. Aircraft*, vol. 60, No 3, May 2023 (online Nov 2022).
2. Bridges, J.E., "Results of the NASA Prediction Uncertainty Reduction Tech Challenge", AIAA Paper 2025-1798, AIAA SciTech Forum, 6-10 January 2025, Orlando, FL.
3. Zaman, K.B.M.Q. and Heberling, B.C., 2021, "A study of flow and noise from supersonic plug nozzles", *AIAA Paper* 2021-2304, Aviation Forum, August 2-6, 2021.
4. Sterbentz, W.H. and Wilcox, F.A., "Investigation of effects of moveable exhaust-nozzle plug on operational performance of 20-inch ram jet", *NACA RM* E8D22, July, 1948.
5. Krull, H. G. and Beale, W. T., "Effect of Plug Design on Performance Characteristics of Convergent-Plug Exhaust Nozzles", *NACA RM* E54HO5, 1954.
6. Berrier, B.L., "Effect of plug and shroud geometry variables on plug-nozzle performance at transonic speeds", *NASA TN D*-5098, March 1969.
7. Angelino, G., "Approximate Method for Plug Nozzle Design", *AIAA J.*, vol. 2 (no. 7), pp. 1834-1835, 1964.
8. Bresnahan, D.L. and Johns, A.L., "Cold flow investigation of a low angle turbojet plug nozzle with fixed throat and translating shroud at Mach numbers from 0 to 2.0", *NASA TM X*-1619, August 1968.
9. Stitt, L.E., "Exhaust nozzles for propulsion systems with emphasis on supersonic cruise aircraft," *NASA RP* 1235, May 1990.
10. Ruf, J. H. and McConnaughey, P.K., "The Plume Physics behind Aerospike Nozzle Altitude Compensation and Slipstream Effect", *AIAA Paper* 97-3217, 33rd Joint Propulsion Conference and Exhibit, Seattle, WA, July 1997.

11. Hagemann, G., Immich, H., and Terhardt, M., “Flow Phenomena in Advanced Rocket Nozzles – The Plug Nozzle,” *AIAA Paper* 98-3522, 34th Joint Propulsion Conference and Exhibit, Cleveland, OH, July 1998.

12. Georgiadis, N.J., DalBello, T.W., Trefny, C.J., and Johns, A. L., “Aerodynamic Design and Analysis of High Performance Nozzles for Mach 4 Accelerator Vehicles”, *AIAA Paper* 2006-16, 44th AIAA Aerospace Sciences Meeting and Exhibit, Reno, Nevada, 2006.

13. Tapee, J. L., “Experimental Aerodynamic Analysis of a Plug Nozzle for Supersonic Business Jet Application”, M.S. Thesis, Purdue University, August, 2009.

14. Maestrello, L., “An Experimental Study on Porous Plug Jet Noise Suppressors”, *AIAA Paper* 79-0673, 5th Aeroacoustics Conference, March 1979.

15. Kibens, V. and Wlezien, R.W., “Noise reduction mechanisms in supersonic jet with porous centerbodies”, AIAA J., *23(5),* pp. 678-684*,* 1985.

16. Das, I.S. and Dosanjh, D.S., “short conical solid/perforated plug-nozzle as supersonic jet noise suppressor”, Journal of Sound and Vibration, 146(3), pp. 391-406, 1991.

17. Chase, J.D, Andres, G., Garzón, G. A. and Papamoschou, D., “Directivity effects of shaped plumes from plug nozzles”, *AIAA Paper* 2013-0008, 51st AIAA Aerospace Sciences Meeting, Grapevine, TX, 2013.

18. Zaman, K.B.M.Q., Fagan, A.F. and Korth, J.H., 2024, “Flow and noise and thrust of supersonic plug nozzles”, *AIAA Paper* 2024-2305, AIAA SciTech 2024 Forum, Orlando, FL., January 8-12, 2024.

19. Bridges, J.E., Podboy, G.G. and Wernet, M.P., “Plug20 Test Report”, *NASA TM* 20210010291, 2021.

20. Bridges, J.E. and Wernet, M.P., “Noise of Internally Mixed Exhaust Systems With External Plug For Supersonic Transport Applications”, *AIAA Paper* 2021-2218, Aviation Forum, August 2-6, 2021.

21. Zaman, K.B.M.Q., Korth, J.H., Fagan, A.F. and Bridges, J.E., 2024, “Study of a plug nozzle for supersonic aircraft concepts”, *AIAA Paper* 2024-3035, AIAA Aeroacoustics Conference, Rome, Italy, June 4-7, 2024.

22. Korth, J.H., “Optimization of Plug Nozzles Using CFD Informed Design Space Querying”, *AIAA Paper* 2024-1776, AIAA SciTech Forum, Orlando, FL, January 8-12, 2024.

23. Korth, J.H., Burt, J.M., Zaman, K.B.M.Q. and Fagan, A., “Investigation of physical mechanisms for jet noise reduction by plug nozzle porosity”, *AIAA Paper* 2025-2163, AIAA SciTech Forum, Orlando, FL, 6-10 January 2025.

24. Shapiro, A.H., “The dynamics and thermodynamics of compressible fluid flow, volume I”, The Ronald Press Company, New York, USA, 1953.

25. Mikkelsen, K. L. and Brasket, R. G., "An Equation Set for ASME Nozzle Discharge and Thrust Coefficients," *AIAA Paper* 2011-1265, Jan. 2011.

26. Zaman, K.B.M.Q., Dahl, M.D., Bencic, T.J. and Loh, C.Y., “Investigation of a ‘transonic resonance’ with convergent-divergent nozzles”, *J. Fluid Mech*., 463, pp. 313-343, 2002.

27. Zaman, K.B.M.Q., Bridges, J.E. and Brown, C.A., “Excess broadband noise observed with overexpanded jets”, *AIAA J.*, 48(1), pp202-214, 2010.

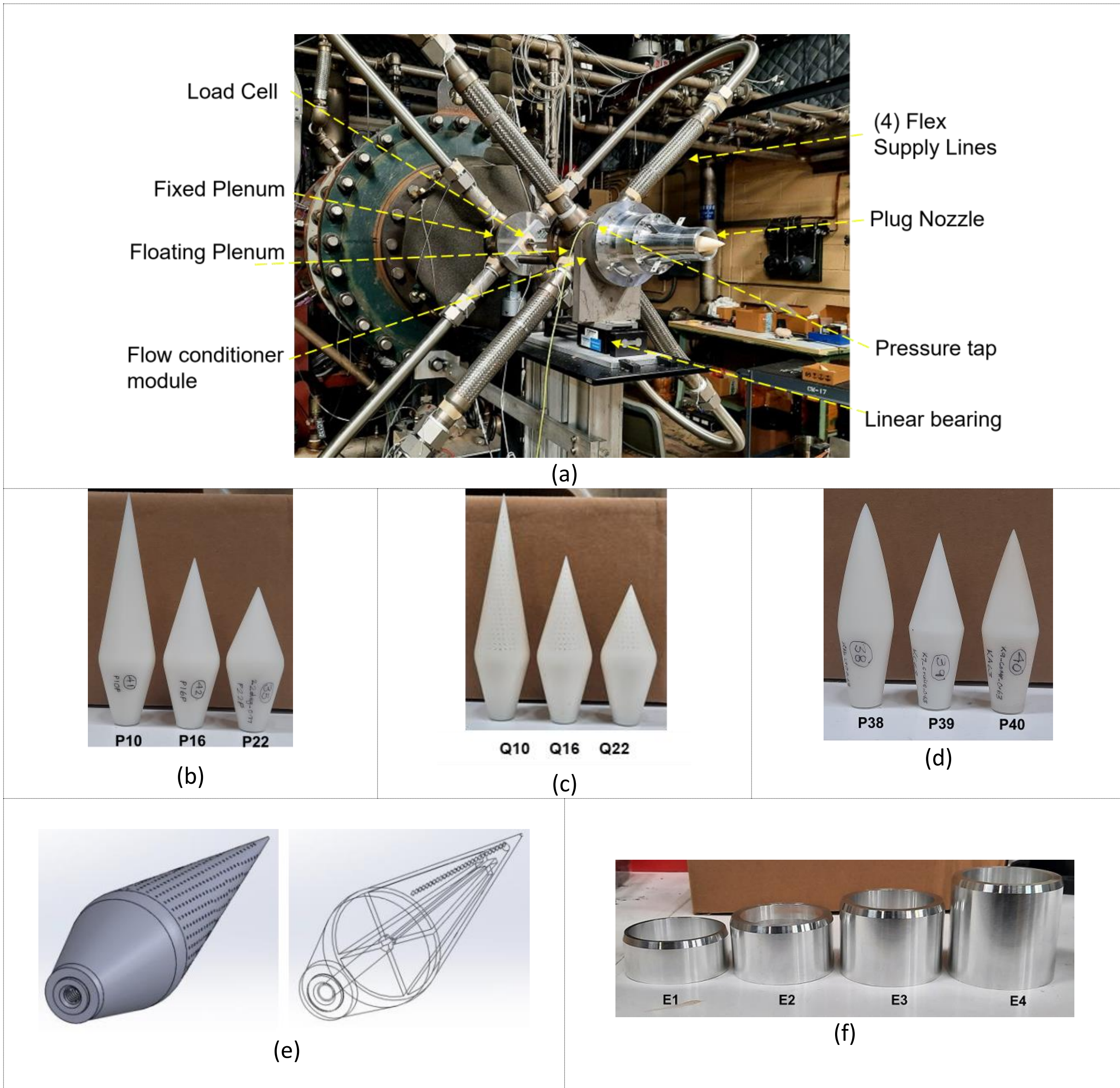

Fig. 1 Experimental Facility. (a) Thrust measurement setup, (b) picture of 3 solid plugs, (c) picture of 3 porous plugs, (d) optimized plugs via numerical study, (e) CAD drawing of a porous plug, (g) picture of nozzle lip extensions.

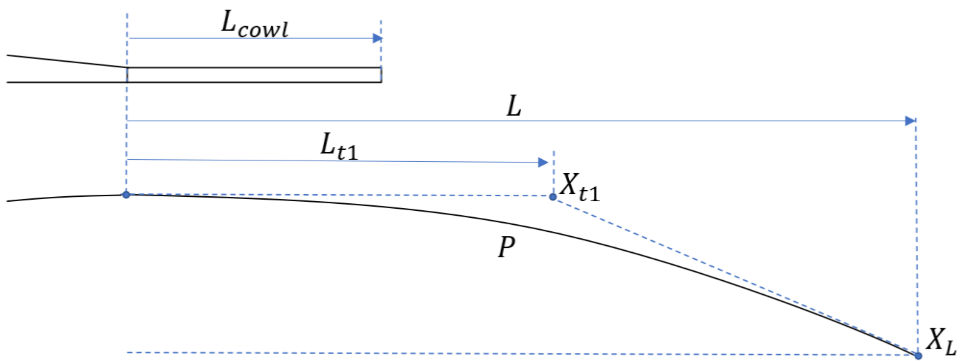

(a)

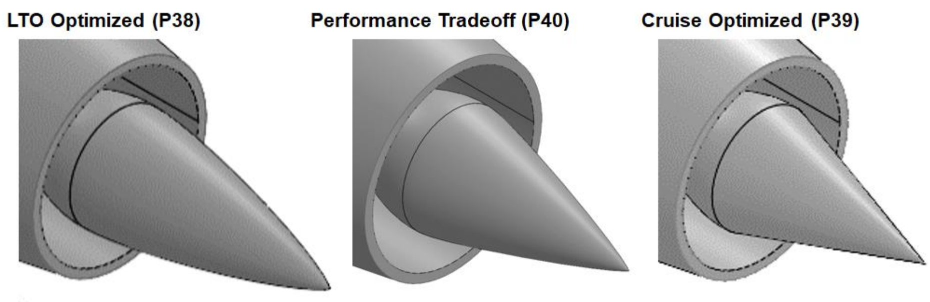

(b)

Fig. 2 Optimization of plug geometry via numerical simulation from [22]. (a) plug parameters varied for optimization, (b) Resultant plug geometries optimized for LTO (left) and cruise (right), as well as a 'compromise' geometry (middle).

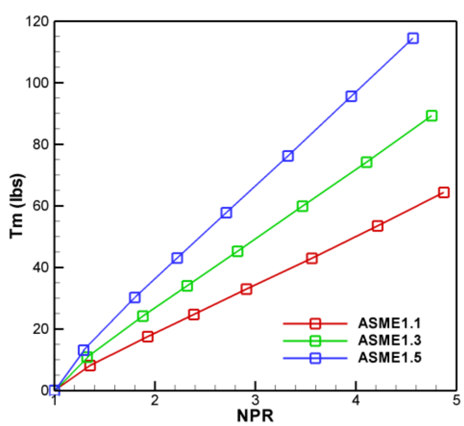

(a)

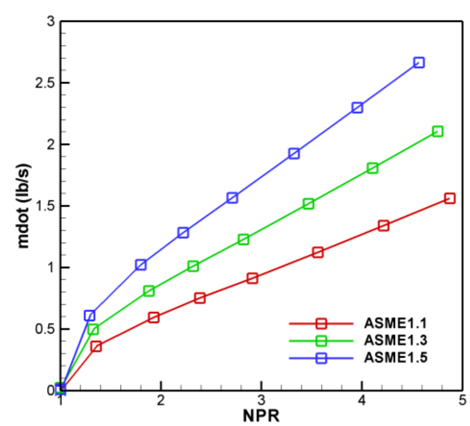

(b)

Fig. 3 Calibration data with three 'ASME' nozzles having diameters of 1.1", 1.3" and 1.5". (a) Measured axial force (*Tm*), (b) measured mass flow rate (*mdot*), as a function of NPR.

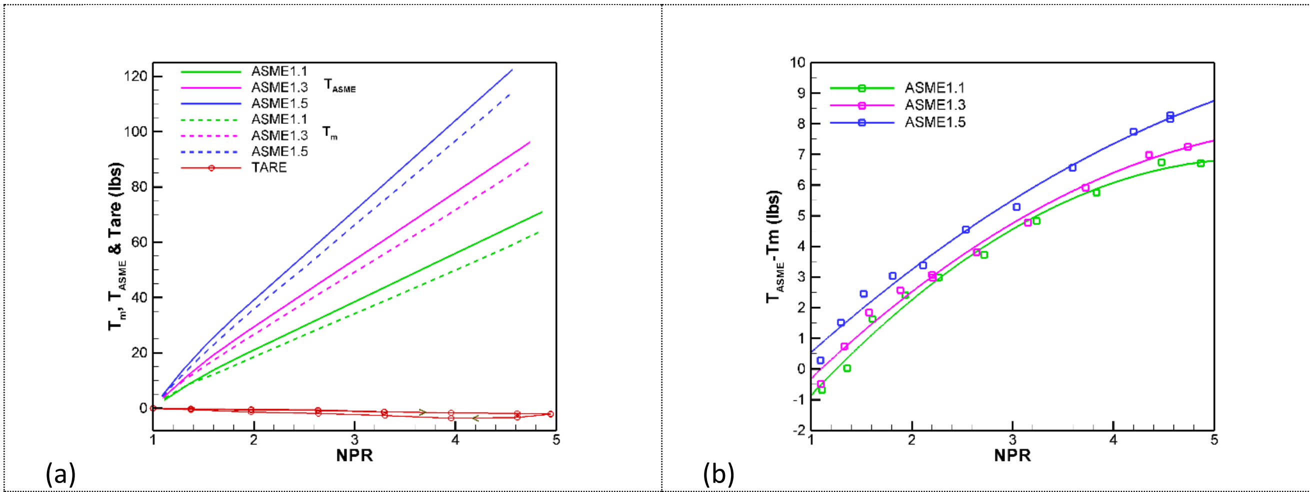

Fig. 4 Force data for three ASME nozzles. (a) Measured force (*Tm*) and calculated actual force (T_{ASME}) shown by solid and dashed lines, respectively; '*Tare*' force (red) for no-flow. (b) Difference (T_{ASME} -*Tm*) for the three nozzles.

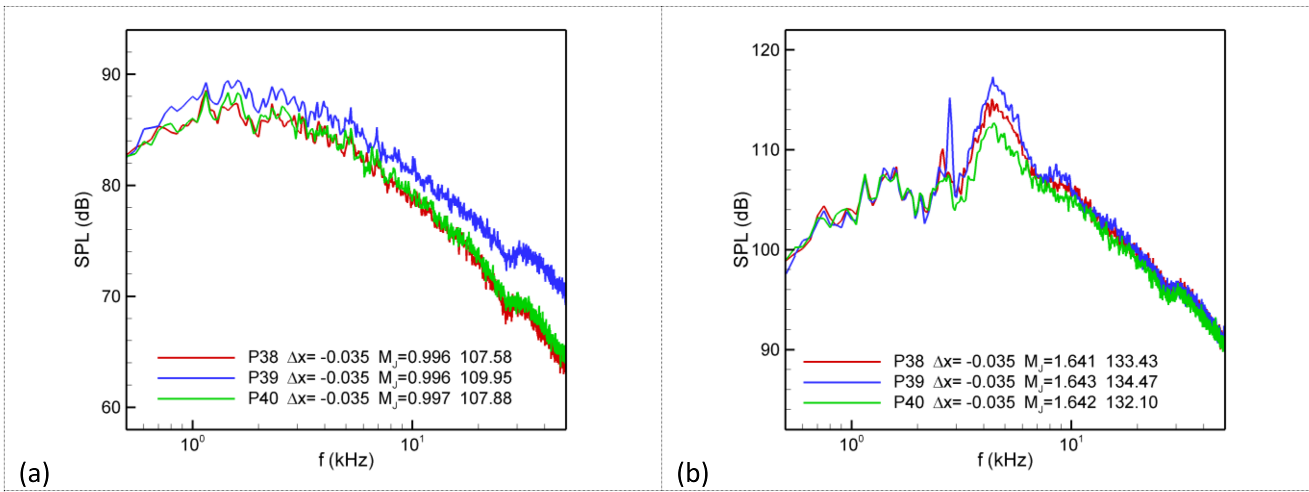

Fig. 5 Sound pressure level (SPL) spectra at θ≈90° for the three optimized plugs; crown location △x= -0.035". Plug case, crown location, jet Mach number and overall sound pressure level (OASPL, dB) are indicated in the legend. (a) M_J ≈1.0, NPR≈1.89, 'LTO' condition, (b) M_J ≈1.65, NPR≈4.6, 'cruise' condition.

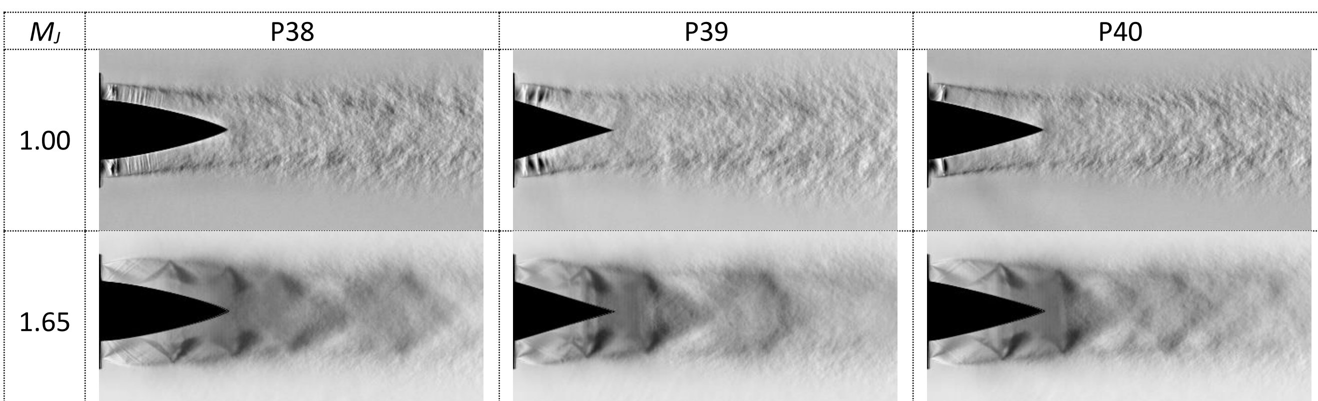

Fig. 6 Schlieren images of flows corresponding to the noise data in Fig. 5

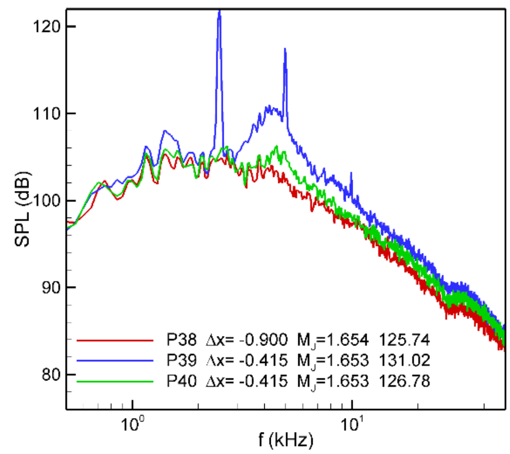

Fig. 7 SPL spectra at θ≈90° for the three optimized plugs: P38 with △x=-0.90” (red lines), P39 with △x=-0.415” (blue lines) and P40 with △x=-0.415” (green lines); M_J = 1.65.

M_J	P38	P39	P40
1.65	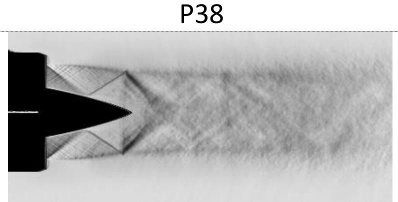	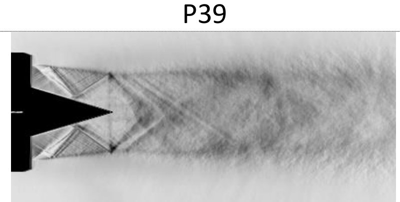	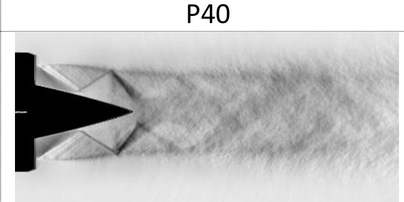

Fig. 8 Time-averaged schlieren images of flows corresponding to the noise data in Fig. 7.

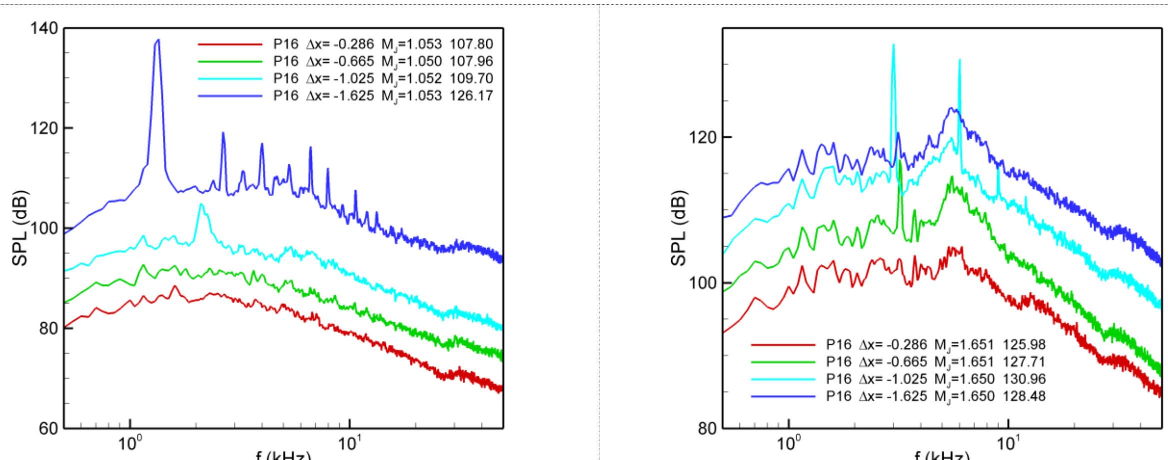

(a) (b)

Fig. 9 SPL spectra for the 16° conic plug (P16) with different extensions (crown locations), E1 (△x=-0.285”), E2 (△x=-0.665”), E3 (△x=-1.025”) and E4 (△x=-1.625”). Successive traces are staggered by 5dB. (a) M_J =1.005 (NPR=1.9) and (b) M_J =1.65 (NPR=4.6).

Extension	M_J =1.005 (NPR=1.9)	M_J =1.650 (NPR=4.6)
E1 (△x=-0.285”)	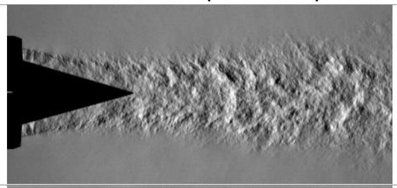	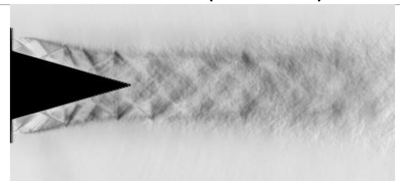
E2 (△x= -0.665”)	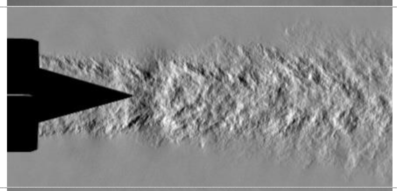	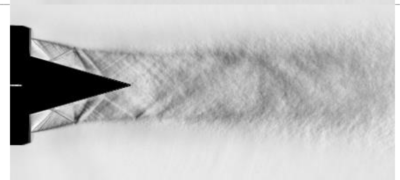
E3 (△x= -1.025”)	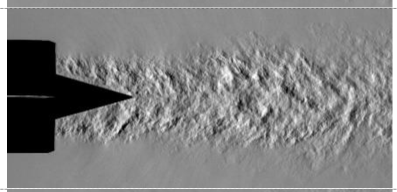	
E4 (△x= -1.625”)	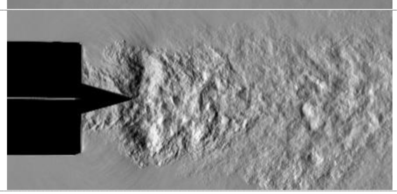	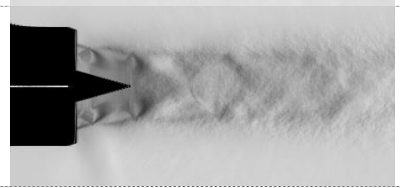

Fig. 10 Schlieren images of flows for the 16° conic plug with different extensions corresponding to the noise data of Fig. 9. For MJ=1 instantaneous images are shown while for M_J =1.65 time-averaged images are shown.

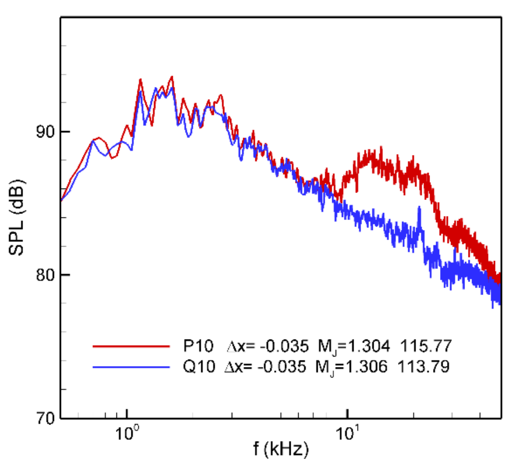

(a)

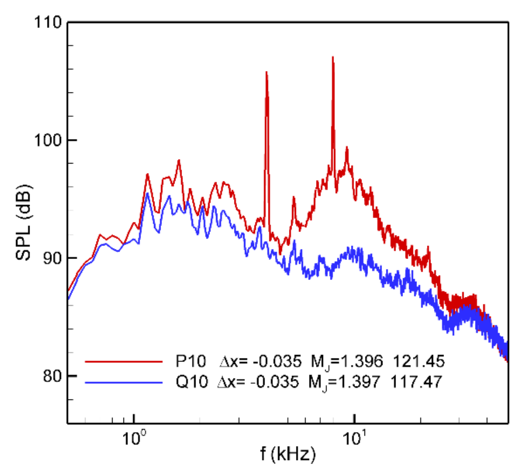

(b)

Fig. 11 Continued next page.

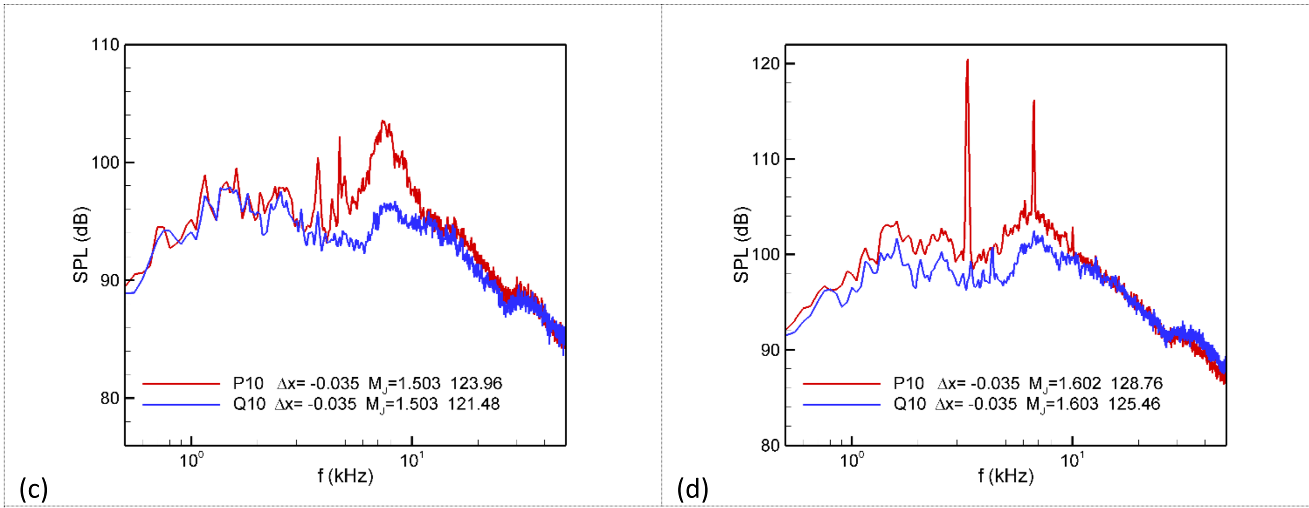

Fig. 11 SPL spectra at θ≈90° for the 10° conic plug showing plug porosity effect. Red lines: solid plug (P10), blue lines: porous plug (Q10).

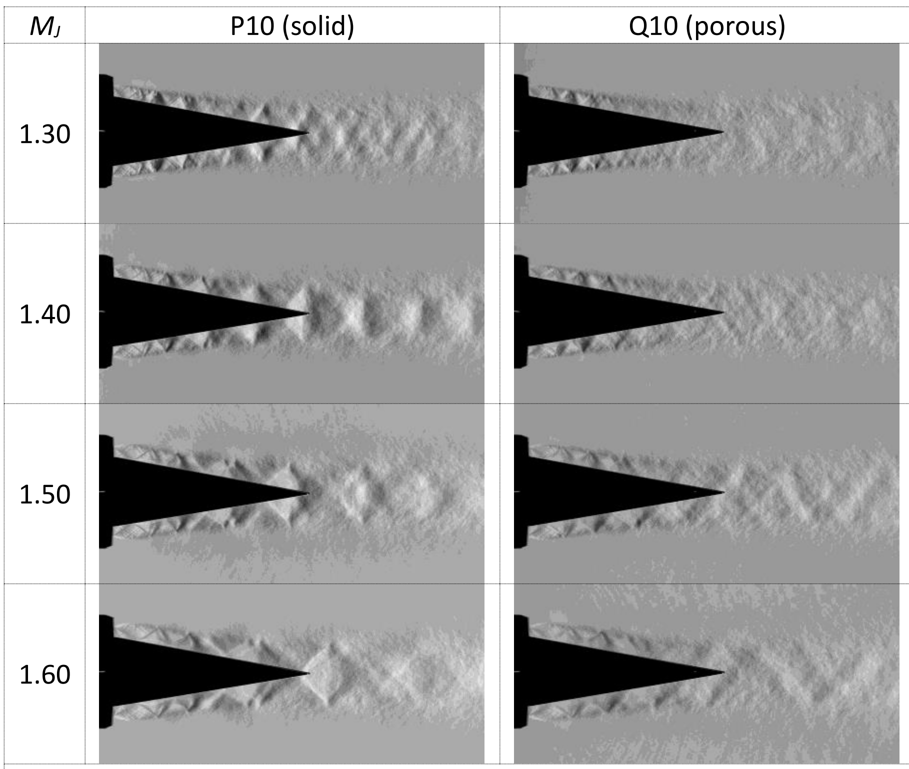

Fig. 12 Time-averaged schlieren images of flows for the 10° conic plug corresponding to the noise data of Fig. 11.

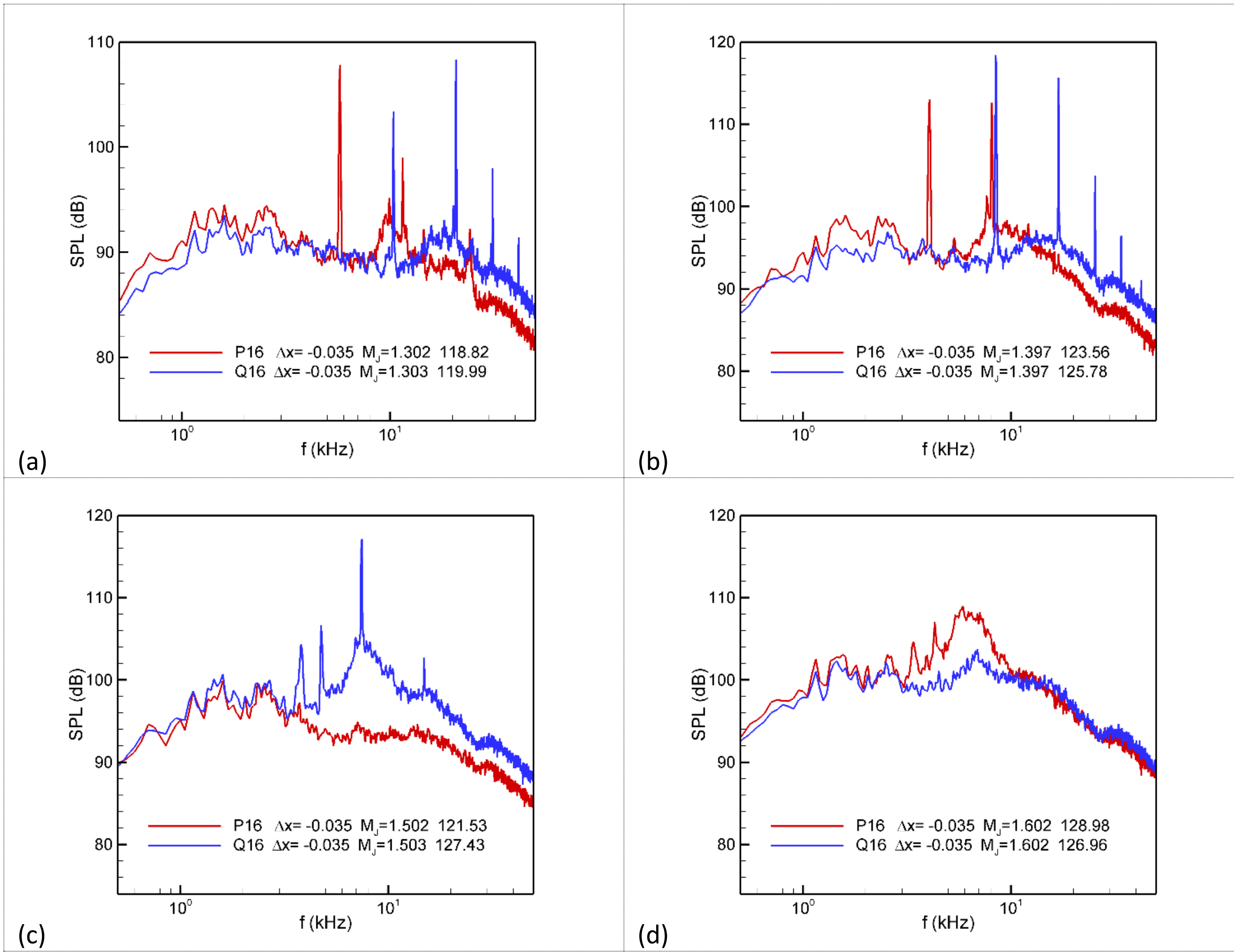

Fig. 13 SPL spectra at θ≈90° for the 16° conic plug showing plug porosity effect. Red lines: solid plug (P16), blue lines: porous plug (Q16).

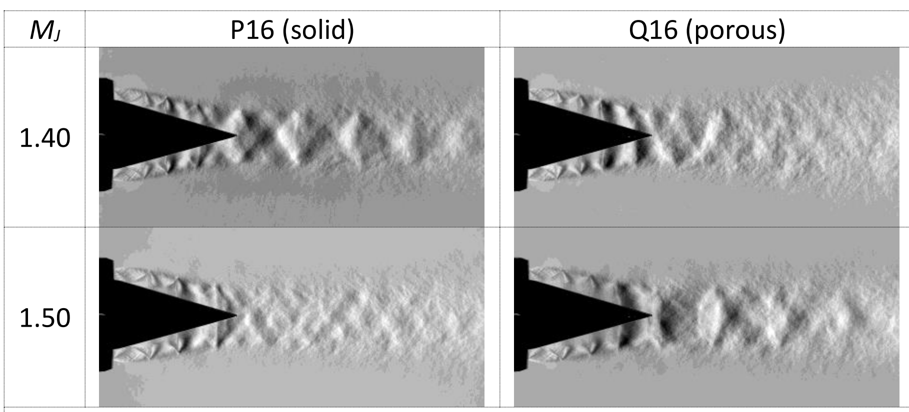

Fig. 14 Time-averaged schlieren images of flows for the 16° conic plug at two values of M_J corresponding to the noise data of Fig. 13.

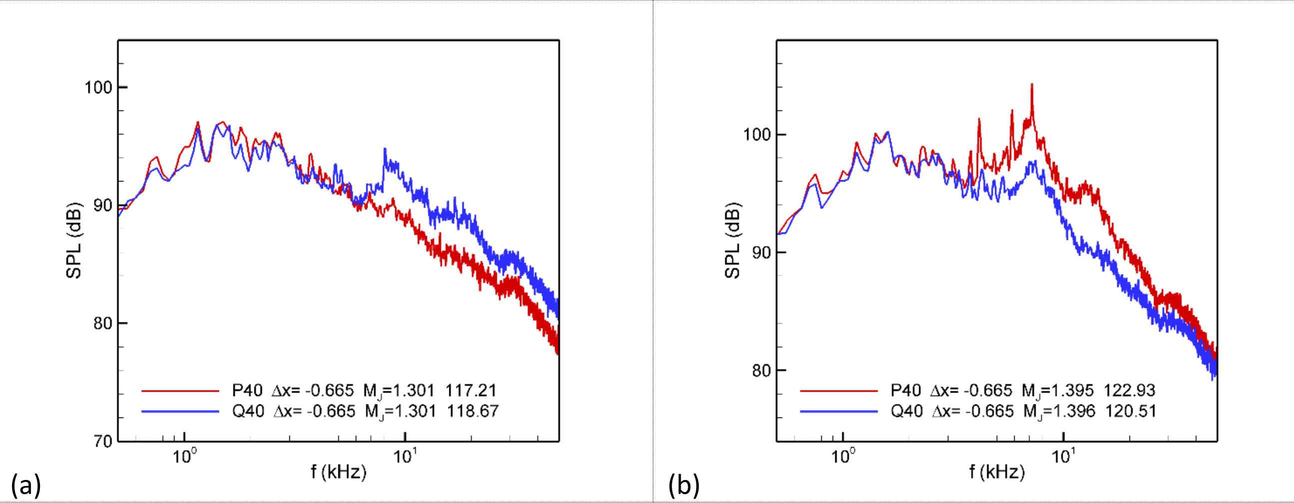

Fig. 15 SPL spectra at θ≈90° for the P40 plug (compromise design) showing plug porosity effect. Red lines: solid plug (P40), blue lines: porous plug (Q40).

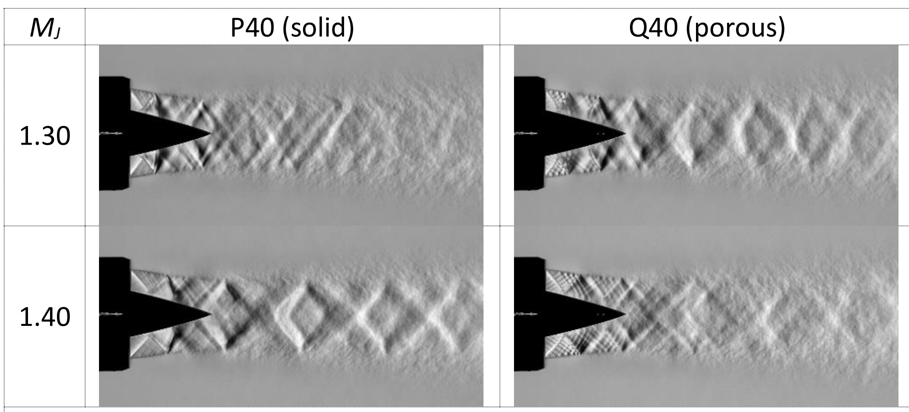

Fig. 16 Time-averaged schlieren images of flows for the 16° conic plug corresponding to the noise data of Fig. 15.

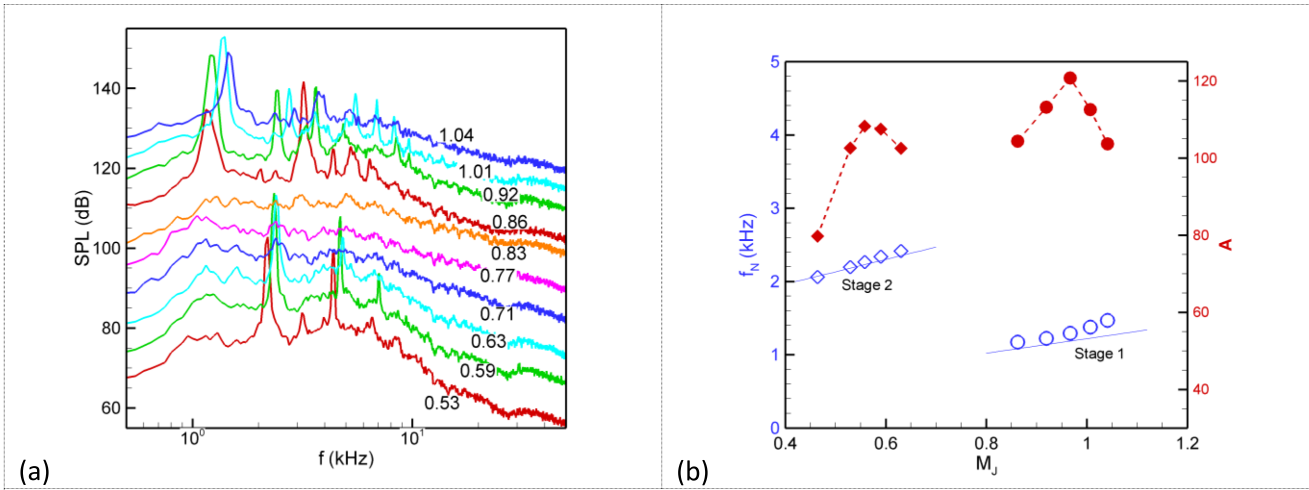

Fig. 17 Characteristics of x-tone for the 10° conic plug (P10) with crown location, △x=-1.625”. (a) SPL spectra at various M_J (successive traces staggered by 5dB, ordinate pertains to trace at bottom), (b) x-tone spectral peak frequency and amplitude as a function of M_J, solid lines prediction by correlation given in [26]; M_J range 0.4-1.2 corresponds to NPR range of 1.12-2.42.

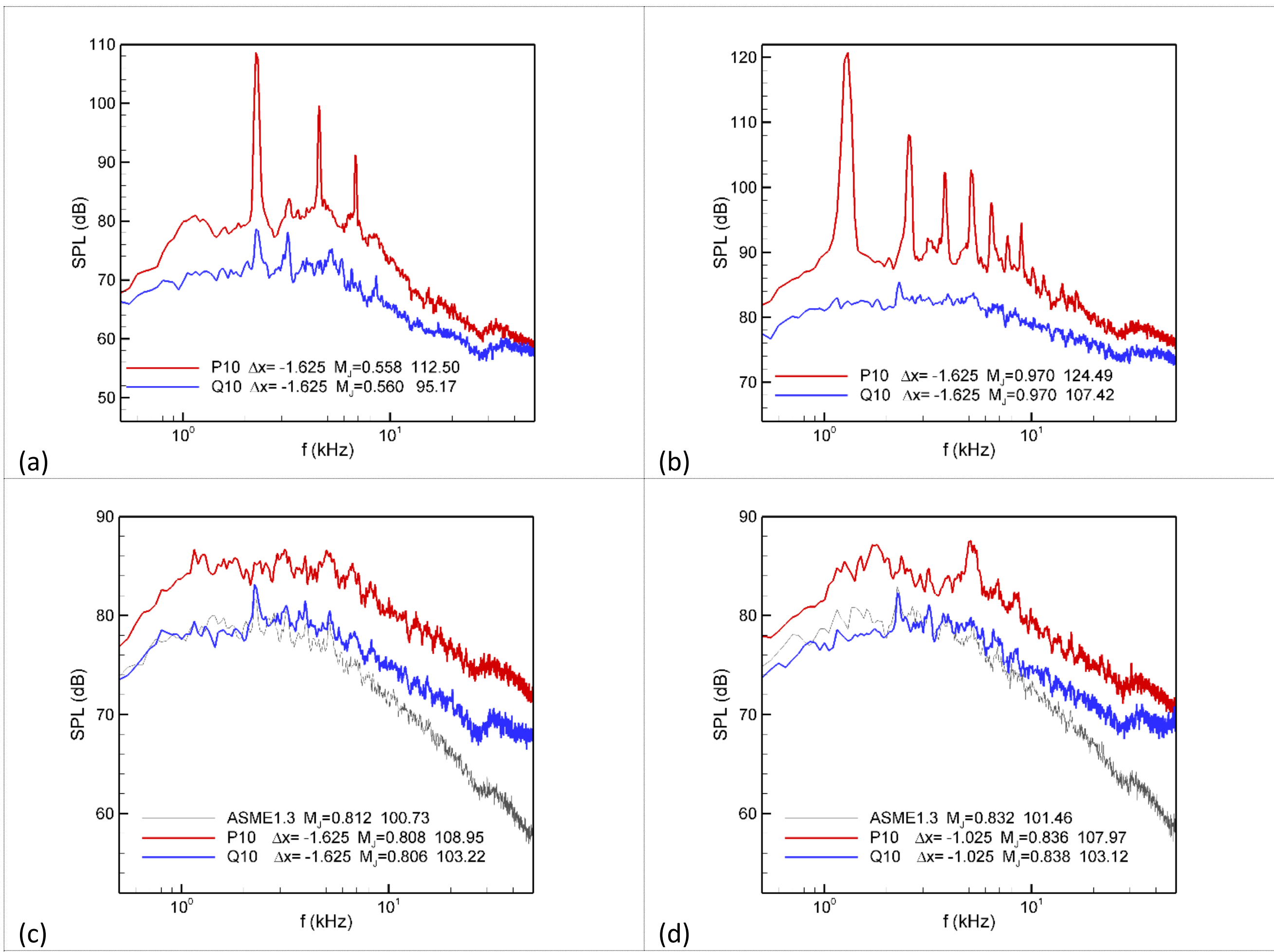

Fig. 18 SPL spectra at θ≈90° for the 10° conic plug demonstrating the effect of plug porosity; red: solid plug (P10), blue: porous plug (PRS6), grey: ASME 1.3” nozzle. (a) M_J =0.59, △x=-1.625” (x-tone), (b) M_J =0.97, △x=-0.1.625” (x-tone), (c) M_J =0.81, △x=-1.625” (EBBN), (d) M_J =0.84, △x=-1.025” (EBBN).

M_J	P10 (solid)	Q10 (porous)
0.59	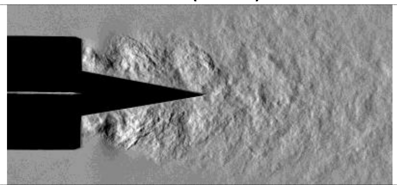	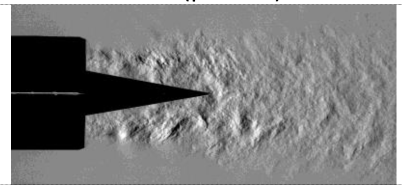
0.97	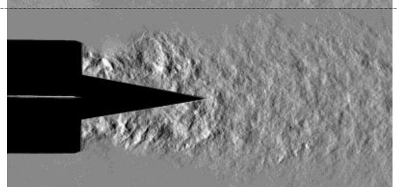	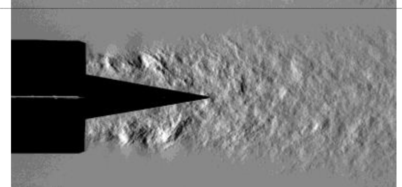
0.81	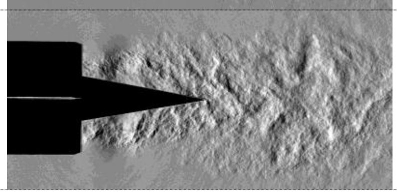	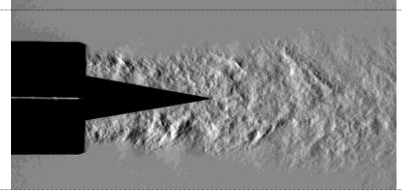

Fig. 19 Instantaneous schlieren images of flows for the 10° conic plug corresponding to the noise data of Fig. 16 (a), (b) and (c); △x=-1.625”

.

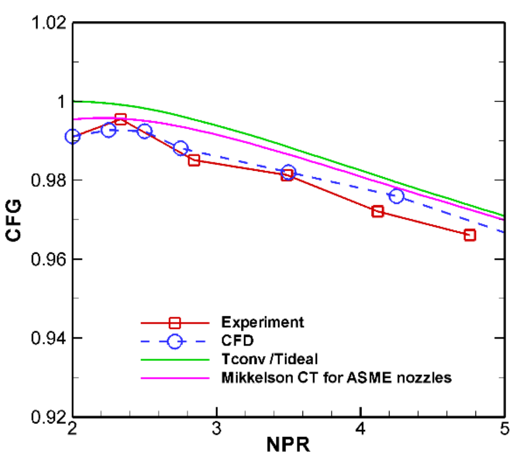

(a)

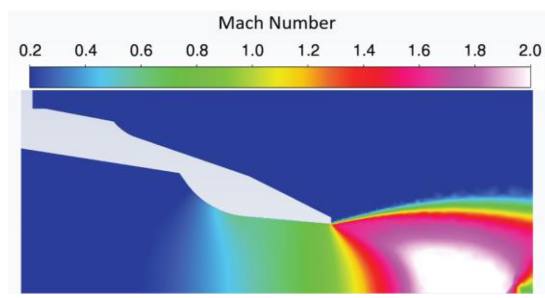

Mach number contours for NPR=4.25.

(b)

Fig. 20 Flow and thrust of D=1.3” ASME nozzle. (a) Thrust coefficient vs. NPR; red line: experimental data, blue dashed line: CFD prediction, green line: analytical prediction, light blue line: correlation for ASME nozzles from [25]. (b) An example of CFD results from which the *CFG* data are obtained, also showing the nozzle geometry.

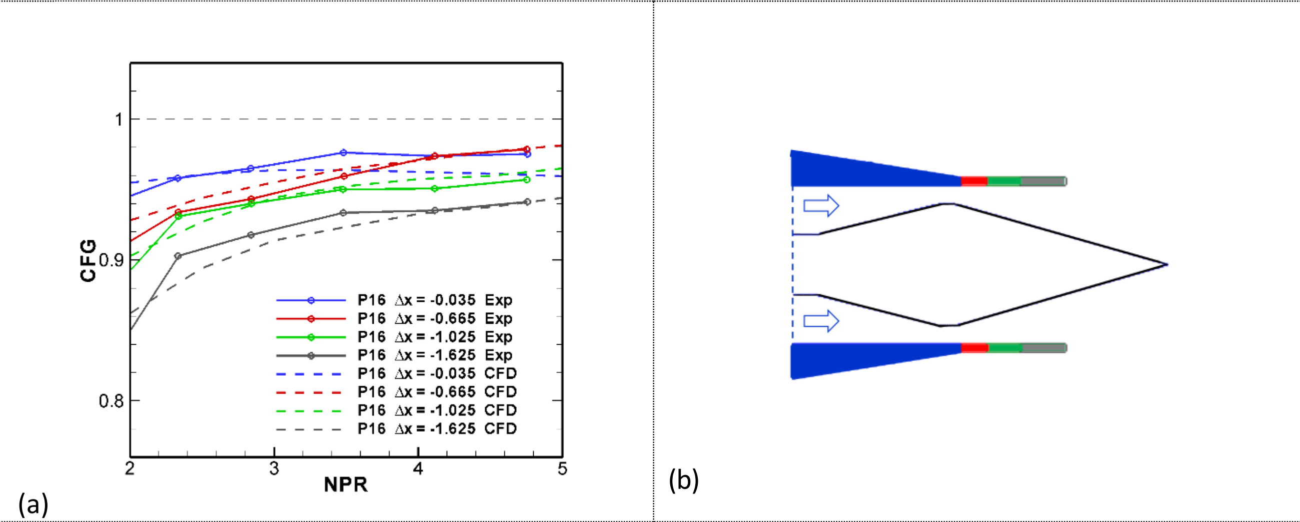

Fig. 21 Thrust coefficient of 16° conic plug for different lip extensions. (a) *CFG* vs. NPR; solid lines: experimental results, dashed lines: CFD results. (b) Schematic of the four lip extensions.

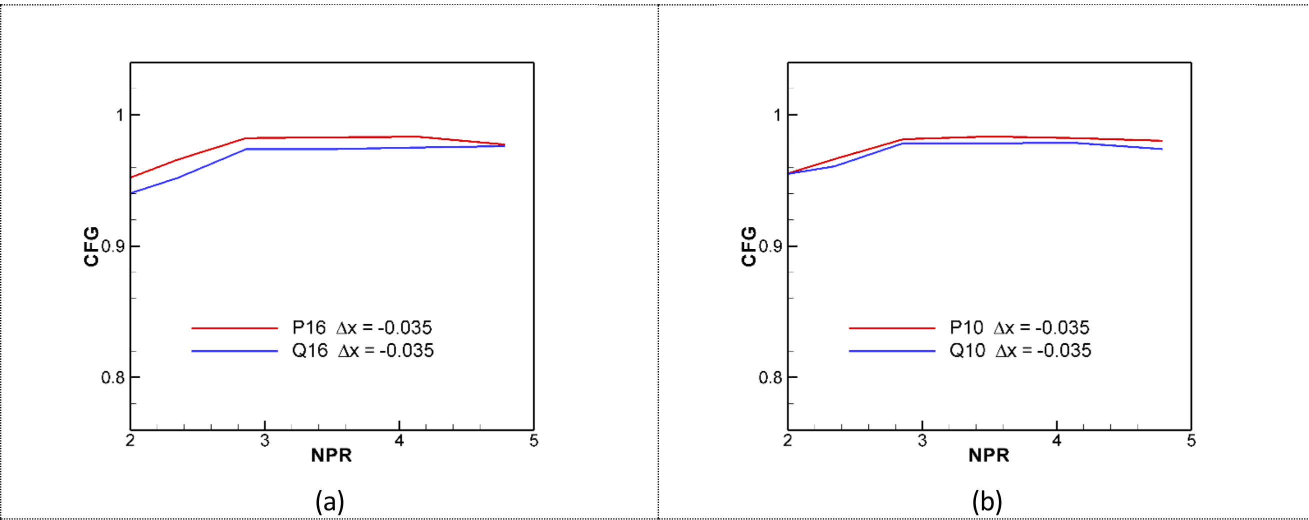

Fig. 22 Experimental results on thrust coefficient vs. NPR showing plug porosity effect. Solid lines are for solid plugs while dashed lines are for corresponding porous plugs. (a) 16° conic case (P16 vs Q16), (b) 10° conic case (P10 vs Q10).